Effect of shear strain on the α–ε phase transition of iron: a new approach in the rotational diamond anvil cell

2006 J. Phys.: Condens. Matter 18 S1075

(http://iopscience.iop.org/0953-8984/18/25/S14)

INSTITUTE OF PHYSICS PUBLISHING JOURNAL OF PHYSICS: CONDENSED MATTER

J. Phys.: Condens. Matter **18** (2006) S1075–S1082 doi:10.1088/0953-8984/18/25/S14

Effect of shear strain on the α–ε phase transition of iron: a new approach in the rotational diamond anvil cell

Yanzhang Ma, Emre Selvi, Valery I Levitas and Javad Hashemi

Department of Mechanical Engineering and Center for Mechanochemistry and Synthesis of New Materials, Texas Tech University, Lubbock, TX 79409, USA

Received 1 December 2005, in final form 24 March 2006
Published 8 June 2006
Online at stacks.iop.org/JPhysCM/18/S1075

Abstract

The effect of shear strain on the iron α–ε phase transformation has been studied using a rotational diamond anvil cell (RDAC). The initial transition is observed to take place at the reduced pressure of 10.8 GPa under pressure and shear operation. Complete phase transformation was observed at 15.4 GPa. The rotation of an anvil causes limited pressure elevation and makes the pressure distribution symmetric in the sample chamber before the phase transition. However, it causes a significant pressure increase at the centre of the sample and brings about a large pressure gradient during the phase transformation. The resistance to the phase interface motion is enhanced due to strain hardening during the pressure and shear operations on iron and this further increases the transition pressure. The work of macroscopic shear stress and the work of the pressure and shear stress at the defect tips account for the pressure reduction of the iron phase transition.

1. Introduction

Iron is one of the most abundant materials in our globe and dominates the Earth's core. Thus the structural properties and physics of iron are important and critical for its application, as well as understanding the interior of the Earth. At ambient conditions, iron has a body centred cubic (bcc) crystal structure. It transforms to a hexagonal close packed (hcp) structure under high pressure [1–4]. Although other phases have also been reported [5–7], the hcp structure is found to be the dominant phase under high pressure and high temperature [8]. In the last few decades, the structural properties of iron have been explored extensively, both experimentally (e.g. [9, 10] and references therein) and theoretically (e.g. [11, 12] and references therein) under high pressure and high temperature.

While most of the previous works emphasize the high-pressure and high-temperature effects of iron, the importance of the elastic and plastic properties has also been recognized (e.g. [13–16]). Several experimental methods have been developed [14, 17–19] to obtain elastic

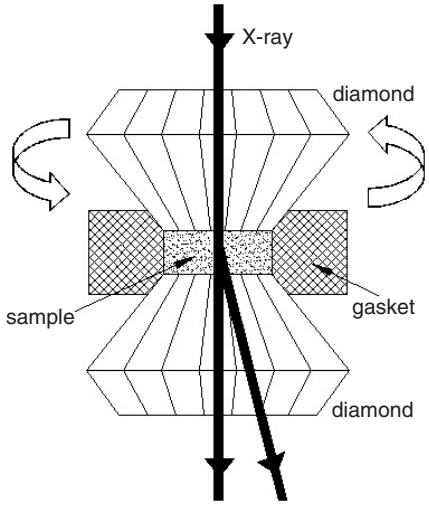

Figure 1. Schematic diagram of the rotational diamond anvil cell, showing the anvils, the sample chamber, and the alignment of the x-ray beam for *in situ* x-ray diffraction measurements.

properties using synchrotron x-ray diffraction based on theoretical calculations [20, 21]. The apparatus used to generate pressure and deformation is either a diamond anvil cell or a modified multi-anvil cell. A diamond anvil cell generates axial compression on the sample chamber if no pressure medium is used or the sample contacts the anvils in the sample chamber. In a modified multi-anvil apparatus, one anvil is designed to translate back and forth to produce deformation on the sample [18]. Another high-pressure apparatus that can generate deformation under pressure is the RDAC [22–27]. As is shown in figure 1, the design of the cell allows rotation of the anvil on the piston side of the piston–cylinder high-pressure apparatus. With the applied load firmly supporting the anvils, the rotation of the diamond anvil produces shear stress and strain on the sample and leads to strong plastic deformation. This, along with the ideal property of diamond (being transparent to a wide range of frequencies), made it possible to fully explore the properties of materials under high pressure and large shear. We successfully utilized the rotational diamond anvil cell in *in situ* x-ray diffraction measurements to study the effect of shear on the phase transformation, the lattice disorder, and transformation-induced plasticity of materials [28–30]. Since the RDAC possesses the advantages of both a diamond cell, being flexible, compact, and light-weight, and the unique function of generating shear stress and strain, we may well expect the rotational diamond anvil to become one of the most powerful methods in the exploration of materials under pressure and shear. In this paper, we present an experimental study of the effect of shear deformation on the α–ε phase transition of iron.

2. Experimental details

Details of the RDAC used, which allows unlimited rotation angle in both directions, can be found in [30]. The culet size of the diamond anvils was 300 μm. In the alignment of the anvils, we kept a small angle (four interference lines) between the two faces of the anvils to generate shear stress effectively. A stainless-steel gasket was pre-indented with a 280 μm hole drilled at the centre. This gasket was used to limit substantially the radial plastic flow of the sample during compression and rotation, which would significantly reduce the thickness of the

sample. It also allowed us to obtain quasi-homogenous pressure in the sample in a certain pressure range. After primary compression, the gasket hole expanded and the sample covered the whole range of the anvil faces. We loaded a very thin layer of fine ruby particles on the face of the bottom anvil, which allowed us to measure the pressure gradient along the radius of the sample plate formed between the anvils. Iron powder with a particle size of between 6–10 μm (Alfa Aesar, 99.5% pure) was tested in our measurements. The sample was hand compacted between hard plates to form a flake, which was loaded into the sample chamber. The pressure was first raised to ∼4.6 GPa (centre position of the sample; the same below, if not specified) before performing rotation. The anvil was then rotated several times, up to a total of 720°. An additional load was added thereafter to raise pressure to 9.6 GPa. Then the anvil was rotated by 180° and 360°, respectively. After each operation (including loading and rotation), the pressure was measured along the diameter of the sample, and x-ray measurements were performed at the centre as well as at the off-centre positions to distinguish the effect of shear from compression. X-ray diffraction measurements were carried out at the high pressure beamline X17C at the National Synchrotron Light Source in Brookhaven National Laboratory. The angle-dispersive imaging plate method was used, with an x-ray wavelength of 0.5340 Å and a beam size of 20 μm × 25 μm. The exposure time was 11 min. After exposure, the image was read using a Fuji Image Reader (BAS-2500) with 100 μm × 100 μm resolution. The integration was performed using Fit2d, written by A P Hammersley.

3. Results and discussion

Figure 2 shows the pressure distribution after each operation. The pressure distribution before rotation had a linear distribution of ∼2–6 GPa. The pressure increased from one end of the sample to the other due to the angle between the faces of the anvils. After a 30° rotation, the pressure increased to 8.8 GPa, an average increase of ∼4 GPa, and the pressure distribution became symmetric. Additional rotation (90°, 180°, 360°, and 720°) did not seem to change the pressure much. The pressure elevation through shear appeared to reach a limit (∼9 GPa). Also, the shear operation made the pressure distribution more uniform. After 720° rotation, the pressure variation was within ∼1 GPa within the whole range of the anvils. This could be ascribed to the dynamical friction between the sample and the diamond faces. As is shown in figure 3 (the patterns from 4.6 GPa and 0° to 8.6 GPa and 720°), there was no phase transition at this stage.

After an additional load was applied, the pressure rose to 9.5 GPa. The pressure divergence caused by the tilt of the anvils became less significant. The centre pressures were slightly higher than the outer region (figure 2). This pressure increase did not initiate the phase transition of iron (figure 3). However, because this pressure was very close to the transition pressure of iron (∼13 GPa [13]), and the rotation afterwards led to a pressure increase in the sample chamber with the centre portion greater than the outer, iron's bcc–hcp (α–ε) phase transformation was induced after shear (figures 3 and 4). As a consequence of this phase transition, a significant pressure gradient was introduced, leading to severe heterogeneity on the sample. The maximum pressure near the centre was increased to 15.4 GPa after 180° and 16.8 GPa after 360°; while pressure at the edge did not display an obvious increase (∼8 GPa, figure 2). The centre pressure gained 5–6 GPa due to the rotation. Again, we found that additional rotation of the anvil after an established condition (after 180°) in the sample chamber did not introduce a significant change in pressure distribution in the sample chamber.

Under non-hydrostatic compression and torsion, the radial pressure gradient on the sample is generally caused by the shear friction stress along the radial direction of the diamond anvils.

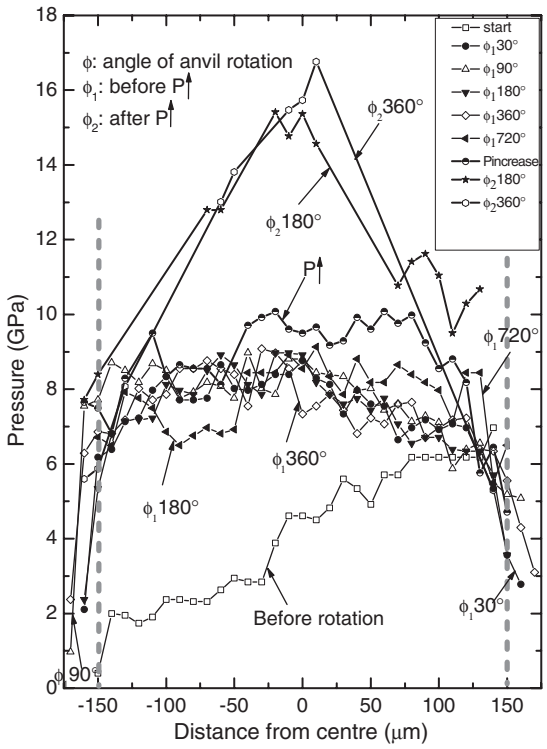

Figure 2. The pressure distribution in the sample chamber along a diameter on the sample plate formed between the diamond anvils. ϕ stands for the accumulated rotation angles of the anvil. ϕ_1 marks those rotation angles after the first compressional load was applied. ϕ_2 indicates those after the second load. $P\uparrow$ means pressure increase by applying load. The grey dashed vertical lines mark the positions of the anvil edges.

It can be expressed through the simplified equilibrium equation:

$$\frac{\partial p}{\partial r} = -\frac{2\tau_r}{h}, \tag{1}$$

where r is the radial distance from the centre of the sample, τ_r is the shear stress along the radial direction, and h is the thickness of the sample. According to this equation, the centre of the sample chamber has higher pressure. Yet, due to the application of a gasket, the flow of the sample can be largely blocked, depending on the strength of the gasket. This was the case in the operation before rotation at 9.5 GPa, where quasi-homogenous pressure distributions were observed. During the anvil rotation at 9.5 GPa, the radial component of the shear friction stress decreases and intense radial plastic flow (in addition to torsion) starts in the entire sample [31, 32]. The flow causes a reduction in sample thickness. This leads to a slight pressure increase at the centre, with a minimum portion of the sample moving away from the anvil faces. As a consequence, a phase transformation may be induced in the centre. In most cases, the high-pressure phase has a higher strength, and hence the shear stress, τ_r, increases during and after the phase transition. Therefore, a larger pressure gradient in the centre is expected during and after the phase transition, according to equation (1). This is the so-called pressure self-multiplication effect that was observed experimentally for other materials [22–30, 33] and was explained theoretically in [31]. The pressure in the centre of the sample, where transformation takes place, increases significantly, depending on the strength of the high-pressure phases. On

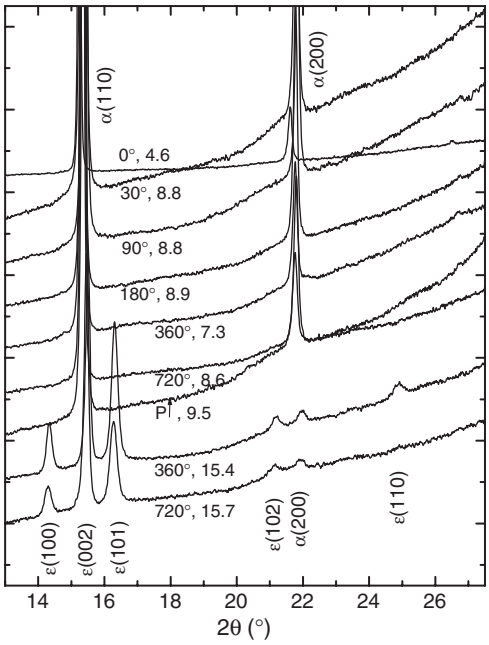

Figure 3. X-ray diffraction pattern of iron in the RDAC after compressional loading and anvil rotation. The degree values are the accumulated rotation angle. The value after the ',' indicates the pressure at the sample centre. $P\uparrow$ means pressure increase by applying load.

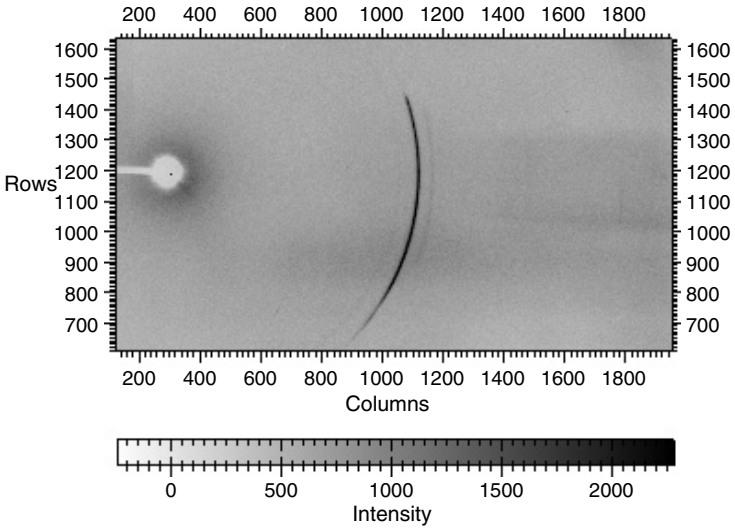

Figure 4. X-ray diffraction image of the iron sample 100 μm away from the anvil centre at 15.4 GPa (centre pressure) after a 360° anvil rotation. The diffraction lines are limited by the opening in the stainless-steel seat for the diamond anvil (a narrow slot with a corn in the centre).

the other hand, the iron α–ε phase transition is accompanied by a large volume reduction, which might cause a pressure decrease when the sample thickness is kept constant. However, under the applied constant loading force and the shear during the rotation, the thickness of the

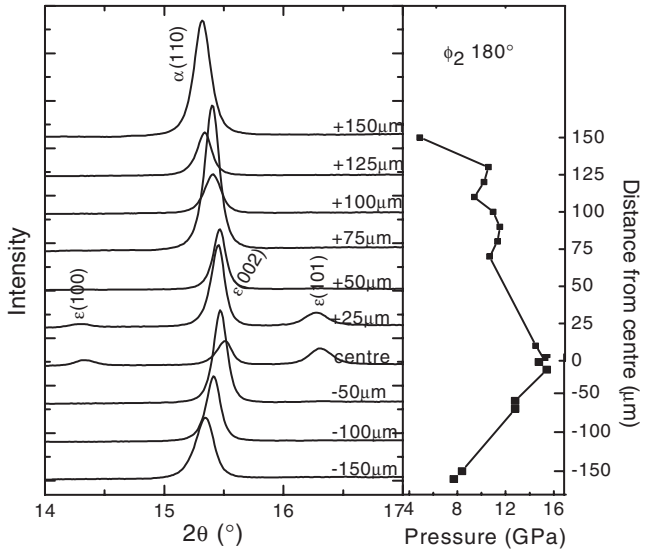

Figure 5. X-ray diffraction patterns after the second compression operation and rotation of 180° at different positions along the diameter of the sample plate, in comparison with pressure distribution at these positions. The values marked on the diffraction patterns indicate the distance from the centre, where the diffraction was taken. The '−' and '+' signs indicate the distances to the left and right sides of sample centre, respectively.

sample will be adjusted (reduced) when the volume in the centre portion is reduced [31]. This compensates the effect of the volume reduction.

Figure 5 shows the x-ray diffraction patterns at different positions, along with their corresponding pressures at those positions after the 180° shear. The (100), (002), and (101) peaks of the iron hcp phase could be observed clearly within a 100 μm range both sides from the centre. These became more intense when they were closer to the centre. The phase concentration of the hcp structure decreased from 100% at the centre to 0% at the edge. Comparing it with the pressure distribution along the radius, we found that the region with hcp phase corresponds to pressures above 10.8 GPa. The maximum pressure was 10.7 GPa in the pure α-phase region. We can thus allocate the initial phase transformation pressure of iron as 10.8 GPa for our conditions. This is much lower than that under a hydrostatic compression: 15.3–15.5 GPa in [34] and 14.9 and 15.3 GPa in [13]. We found no diffraction from α-phase at the centre, which was at 15.4 GPa, from figure 4. The transition was observed to have reached completion at this pressure, where the transition normally starts in hydrostatic compression [34]. Earlier studies of the non-hydrostaticity effect on the α–ε transition of iron indicated that the shear strength of the pressure medium systematically decreased the transition pressure and the interval of the $\alpha \rightarrow \varepsilon$ and $\varepsilon \rightarrow \alpha$ transition [13]. Since the shear operation in our experiments caused significant plastic flow of the sample, indicating that the maximum elastic strain in the sample had been achieved, the initial transition pressure can be considered as the lower boundary of iron under pressure and shear. In fact, the limit (10.6 ± 0.4 [13]) had been reached when Al_2O_3, which was much stiffer than iron, was used as a medium in non-hydrostatic compression.

The iron α–ε transition is a martensitic [35] (displacive) transition. It was pointed out that the hcp phase can be derived from the bcc phase through a minor distortion, in which alternate bcc (110) planes translate in the $[1\bar{1}0]$ direction. In the mean time, the (002) interplanar spacing

is reduced to form the hcp $(1\bar{2}0)$ plane, while the bcc $(1\bar{1}0)$ interplanar distance is enlarged to form the hcp (100) plane [35, 36].

In the compression and shear operation, the maximum macroscopic shear stress, τ, is limited by the yield strength in shear $\tau_y = \sigma_y/2$, where σ_y is the yield strength in compression. The yield strength of iron can be estimated on the basis of data for ultra-low carbon steel (Armco iron); this grows with strain from approximately 0.2 GPa in an annealed state to approximately 1 GPa in the maximally hardened state after experiencing logarithmic plastic strain greater than 100% [32]. The volumetric strain for the α–ε phase transformation is derived to be $\varepsilon_0 \approx 0.1$, while the maximum shear strain is $\gamma \approx 2\varepsilon_0$. Using the expression for the transformation work, $W = p\varepsilon_0 + \tau\gamma$, the contribution of shear stress, $\tau\gamma = 2\tau_\gamma\varepsilon_0 = \sigma_\gamma\varepsilon_0 = 1\varepsilon_0$ GPa, is equivalent to an extra pressure of 1 GPa at its maximum. Consequently, macroscopic shear stress cannot reduce the phase transformation pressure from its equilibrium pressure, 13 GPa [13], to 10.8 GPa and some additional mechanisms have to contribute to the pressure reduction.

There are basic differences between the plastic *strain-induced* phase transformations under high pressure and *stress-induced* phase transformations under hydrostatic and nonhydrostatic loadings [28, 29, 31, 33]. Both pressure- (under hydrostatic conditions) and stress-induced phase transformations (under nonhydrostatic conditions) are initiated predominantly at pre-existing defects (stress concentrators) when the intensity of external stresses does not exceed the macroscopic yield limit. Thus the number of nucleation sites is limited. Therefore, pressure needs to be increased to activate the existing defects with less potential. Strain-induced phase transformation occurs by nucleation at new defects, which are permanently generated during plastic flow. In the strain-induced transition, both pressure and shear stress concentration near the defects contribute to the driving force for the phase transformation and thus contribute to the overall phase transformation kinetics, which consequently lowers the external transition pressure. Furthermore, stress singularity near the defect effectively reduces the nucleation barrier that comes from surface energy, which may lead to a barrierless nucleation without the requirement of thermal fluctuations in the stress-induced transition. This, in fact, is strain-controlled rather than time-controlled kinetics. The direct contribution of the macroscopic shear stress to the transformation work is relatively small, since the macroscopic shear stress is limited by the yield strength in shear. In contrast, the maximum shear stress at the tip of a defect is limited by the theoretical shear strength only, which is two to three orders of magnitude higher than the macroscopic yield strength. In our experiments, both the work of macroscopic shear stresses and of extra pressure and shear stress at the defect tip contributed to the reduction in the transformation pressure.

On the other hand, the dissipative resistance to the interface motion (and, consequently, pressure hysteresis for the direct and reverse phase transformation) is proportional to the yield strength σ_y [31, 32]. The plastic shear operation before phase transformation in our experiments also significantly increases the strength of iron due to strain hardening, which increases the transition pressure. The observed transition pressure in our experiments is thus a compromised effect.

4. Conclusion

We have studied the iron α–ε phase transition under pressure and shear in an RDAC. The shear operation leads to a pressure elevation and a more symmetrical distribution between the anvils without phase transition. During the phase transformation, the pressure at the centre of the sample chamber can be increased substantially, together with the creation of large pressure heterogeneity. We found the lower bound of the phase transition to be 10.8 GPa. Complete

phase transformation was observed at 15.4 GPa. The plastic strain generated during the anvil rotation significantly reduces the initial transformation pressure. The main reason for the reduction is the nucleation of iron ε-phase at the defects (stress concentrators) permanently generated during the plastic flow. The observed reduction is a balance between the work of the macroscopic shear stress, the work of the local pressure and shear stress at the strain-induced defect tips, and the increased resistance to the phase interface motion generated during the pressure and shear operations.

Acknowledgments

Thanks are due to William Bassett for his comments and advise on our manuscript. This project was supported by the Texas Tech University Start-up fund and the Texas Tech Excellence fund. This work is supported by DOE under agreement number DE-FC03-03NA00144.

References

[1] Bancroft D, Peterson E L and Minshall S 1956 *J. Appl. Phys.* **27** 291
[2] Jamieson J C and Lawson A W 1962 *J. Appl. Phys.* **33** 776
[3] Johnson P C, Stein B A and Davis R S 1962 *J. Appl. Phys.* **33** 557
[4] Takahashi T and Bassett W A 1964 *Science* **145** 483
[5] Saxena S K, Dubrovinsky L S, Haggkvist P, Cerenius Y, Shen G and Mao H K 1995 *Science* **269** 1703
[6] Yoo C S, Akella J, Campbell A J, Mao H K and Hemley R J 1995 *Science* **270** 1473
[7] Andrault D, Fiquet G, Kunz M, Visocekas F and Hausermann D 1997 *Science* **278** 831
[8] Ma Y Z, Somayazulu M, Shen G, Mao H K, Shu J F and Hemley R J 2004 *Phys. Earth Planet. Inter.* C **143/144** 455
[9] Shen G, Mao H K, Hemley R J, Duffy T S and Rivers M L 1998 *Geophys. Res. Lett.* **25** 373
[10] Mao H K *et al* 2001 *Science* **292** 914
[11] Anderson O L and Isaak D G 2000 *Am. Mineral.* **85** 376
[12] Alfè D, Price G D and Gillan M J 2002 *Phys. Rev.* B **65** 165118
[13] Bargen N V and Boehler R 1990 *High Pressure Res.* **6** 133
[14] Mao H K, Shu J F, Shen G, Hemley R J, Li B and Singh A K 1998 *Nature* **396** 741
[15] Merkel S, Wenk H R, Gillet P, Mao H K and Hemley R J 2004 *Phys. Earth Planet. Inter.* **145** 239
[16] Wenk H R, Matthies S, Hemley R J, Mao H K and Shu J 2000 *Nature* **405** 1044
[17] Weidner D J, Chen J, Xu Y, Wu Y, Vaughan M T and Li L 2001 *Phys. Earth Planet. Inter.* **127** 67
[18] Wang Y, Durham W B, Getting I C and Weidner D J 2003 *Rev. Sci. Instrum.* **74** 3002
[19] Matthies S, Merkel S, Wenk H R, Hemley R J and Mao H K 2001 *Earth Planet. Sci. Lett.* **194** 201
[20] Singh A K 1993 *Appl. Phys. Lett.* **73** 4278
[21] Singh A K and Balasingh C 1994 *J. Appl. Phys.* **75** 4956
[22] Novikov N V, Polotnyak S B, Shvedov L K and Levitas V I 1999 *J. Superhard Mater.* **21** 36
[23] Blank V D, Boguslavski Y Y, Eremetz M I, Izkevich E S, Konyaev Y S, Shirokov A M and Estrin E I 1984 *JETP* **87** 922
[24] Alexsandrova M M, Blank V D, Golobokov A E, Konyaev Y S and Estrin E I 1987 *Solid State Phys.* **29** 2573
[25] Alexandrova M M, Blank V D and Buga S G 1993 *Solid State Phys.* **35** 1308
[26] Serebryanaya N R, Blank V D and Ivdenko V A 1995 *Phys. Lett.* A **197** 63
[27] Blank V D *et al* 1994 *Phys. Lett.* A **188** 281
[28] Levitas V I, Hashemi J and Ma Y Z 2004 *Europhys. Lett.* **68** 550
[29] Levitas V I, Ma Y Z and Hashemi J 2005 *Appl. Phys. Lett.* **86** 071912
[30] Ma Y, Leviatas V and Hashemi J 2006 *J. Phys. Chem. Solids* at press
[31] Levitas V I 2004 *Phys. Rev.* B **70** 184118
[32] Levitas V I 1996 *Large Deformation of Materials with Complex Rheological Properties at Normal Temperature and Pressure* (New York: Nova Science)
[33] Levitas V I, Ma Y, Hashemi J, Holtz M and Guven N 2006 *J. Chem. Phys.* at press
[34] Zou G, Bell P M and Mao H K 1981 *Carnegie Insti. Washington Yearbook* vol 80, p 272
[35] Bassett W A and Huang E 1987 *Science* **238** 780
[36] Mao H K, Bassett W A and Takahashi T 1967 *J. Appl. Phys.* **38** 272